RSC Advances

PAPER

View Article Online
View Journal | View Issue

Cite this: *RSC Adv.*, 2025, **15**, 40501

Novel aminothiazole-supported chlorocellulose composite for the efficient removal of cationic dyes from wastewater

Abdelrahman S. El-Zeny,[a] El-Sayed R. H. El-Gharkawy,[a] Tarek A. Gad-Allah[b] and Magda A. Akl *[a]

This study aimed at synthesizing a fast-responsive chemically modified cellulose (MC) adsorbent for removing organic pollutants, such as cationic dyes, namely, methylene blue (MB), crystal violet (CV), brilliant green (BG), and malachite green (MG), from wastewater. The MC adsorbent was prepared by the chlorination of cellulose using phosphorous oxychloride ($POCl_3$) to produce chlorodeoxy–cellulose (cellulose–Cl), followed by the nucleophilic attack of 2-(2-aminothiazol-4-yl)acetohydrazide. The prepared material was characterized extensively. The adsorption of dyes onto MC was investigated, individually and in a mixture, in a batch mode under variable experimental conditions, such as pH, contact time, initial dye concentration, temperature, and adsorbent dose, to optimize the adsorption process. From the kinetic investigations, with high R^2 values and lower error functions ((χ^2), (SSE), and (MSE)), the adsorption of MB and CV dyes matched well with the pseudo-second-order kinetic model, while the adsorption of BG and MG dyes matched well with the pseudo-first-order kinetic model. In addition, the Temkin model best fitted the adsorption isotherm data for MB, CV, and BG, while the adsorption data of the MG dye fitted well with the Langmuir isotherm model, with the maximum adsorption capacities of 173.00 mg g^{-1}, 171.80 mg g^{-1}, 188.60 mg g^{-1}, and 82.17 mg g^{-1} for MB, CV, BG, and MG, respectively, at 308 K. Thermodynamic studies revealed the spontaneous and exothermic nature of the adsorption of these cationic dyes onto MC. The MC adsorbent exhibited good recycling performance. After five regeneration and adsorption cycles, the MC adsorbent still had a removal effect greater than 90% for the studied dyes, which indicated its high structural stability. The prepared MC was successfully applied for the removal of cationic dyes from real water samples and synthetic mixtures, with a recovery (*R*%) of higher than 97%. The adsorption mechanism of MB, CV, BG, and MG onto the adsorbent was elucidated. Ultimately, this study demonstrated that the fast-responsive MC adsorbent can be effectively utilized to eliminate MB, CV, BG, and MG cationic dyes from a wide range of real water sources. Collectively, the results indicated that the as-prepared MC adsorbent is promising for cationic pollutant adsorption, and our mechanistic results are of guiding significance for environmental cleanup. This work contributes significantly to understanding how experimental conditions influence the mechanism of MB, CV, BG, and MG dye adsorption by the MC adsorbent, offering valuable and new insights for future applications and optimizations in the treatment of effluent-containing cationic species.

Received 5th May 2025
Accepted 5th August 2025

DOI: 10.1039/d5ra03131a

rsc.li/rsc-advances

1. Introduction

One of the main issues faced in the twenty-first century is the availability of water of a recognized quality. Because of numerous anthropogenic activities, unplanned urbanization, and growing industrialization, the quality of water resources is deteriorating every day. Water pollution, caused by different industries, involves several contaminants like pesticides, heavy metals, dyes, and antibiotics.[1]

Dyes are major constituents of wastewater produced by many industries, including textile, paint, varnish, ink, plastic, pulp and paper, cosmetics, tannery, and dye-producing industries.[2] These wastewaters represent a major threat to the environment because many dyes are noxious and carcinogenic.[3] The complicated structures of dyes prohibit their natural degradation in water streams, leading to the accumulation of dyes in the aquatic environment. As a result, removing dyes from the environment is highly demanded. Several approaches have been investigated for the removal of dyes from aqueous systems. Adsorption, photodegradation, coagulation–

[a]*Department of Chemistry, Faculty of Science, Mansoura University, Mansoura, 35516, Egypt. E-mail: magdaakl@yahoo.com*
[b]*Water Pollution Research Department, National Research Centre, 33 El Buhouth St., Dokki, Giza, 12622, Egypt*

flocculation, chemical oxidation, electrochemical oxidation, biological processes, and other methods have been investigated.[4] Among these, adsorption is considered more favorable than other methods because it is easy to use, inexpensive, highly effective, and suitable for large-scale systems.[5] The development of effective adsorbents is a critical aspect for achieving better performance. Many materials, including chitosan, activated carbon, clay, cellulose-based materials, nano-sized metal oxides, and metal–organic frameworks, have been used as adsorbents.[6]

Cellulose is a polymer found in nature that offers numerous benefits, such as cost-effectiveness, ready availability, reusability, and environmental sustainability. It can be made from a variety of natural sources, including cotton, bamboo, and straw. Due to the absence of functional groups, its adsorption efficiency is comparatively low. To improve its adsorption efficiency, cellulose is chemically modified by introducing new functional groups *via* esterification, grafting, oxidation, halogenation, or etherification.[6–8] One of the most researched approaches involves first synthesizing a halogen derivative by adding it to the original polymeric structure at position C6 in cellulose. The preferred halogen order for this purpose is chlorine > bromine > iodine > fluorine. In order to transfer this element to the cellulosic polymeric chain, the efficacy of the chlorination route has been investigated through the use of various precursor chemicals, such as thionyl chloride, phosphoryl oxychloride, *N*-chlorosuccinimide, and tosyl chloride.[9]

Deoxycelluloses are modified forms of cellulose, in which the hydroxyl groups have been replaced completely or partially by other functional groups. Halodeoxycelluloses are intriguing substances because it is simple to substitute other groups for the halogen. Phosphorous oxychloride's chlorination of cellulose in DMF produces 6-chloro-6-deoxycellulose as a result of preferential functionalization at the sixth carbon.[10]

Functionalizing chlorodeoxycellulose *via* the nucleophilic attack of 2-(2-aminothiazol-4-yl)acetohydrazide for dye removal is an intriguing approach, especially for water treatment and purification. The functionalization of chlorodeoxycellulose with a group like 2-(2-aminothiazol-4-yl)acetohydrazide can help enhance the material's adsorptive properties, making it more efficient at capturing and removing various types of dyes from aqueous solutions. The 2-(2-aminothiazol-4-yl)acetohydrazide group consists of a thiazole ring (which has nitrogen and sulfur atoms) and a hydrazide group (–C(=O)NH–NH_2). The thiazole group is known for its ability to interact with various organic molecules, including dyes, due to its aromatic structure and nitrogen–sulfur heteroatoms. The hydrazide group can potentially form strong interactions with dyes, especially those with functional groups like carbonyls or amino groups, improving adsorption *via* hydrogen bonding, electrostatic interactions and/or π–π interactions.[11–14]

The functionalized cellulose derivatives may be used for water purification, as stationary phases in chromatography, as ion exchangers, and for cation removal such as dyes.[15] Based on the aforementioned information, the objectives of the current study are summarized in the following points:

(i) To design and synthesise a modified cellulose (MC) adsorbent for the adsorption of CV, MB, BG, and MG cationic dyes in single and mixed solutions.

(ii) To characterize MC using elemental analysis, SEM, EDX, FTIR, XRD, TEM, BET and ^{1}HNMR and performances.

(iii) To conduct batch sorption experiments utilizing CV, MB, BG, and MG as pollutants.

(iv) To investigate the ideal parameters required for the optimal adsorption of the studied metal ions, *e.g.*, pH, temperature, the initial concentration of the three investigated metal ions, the mass of MC, the oscillation time, and the ionic strength.

(v) To study the various adsorption isotherms, kinetics, and thermodynamic parameters.

(vi) To comparatively evaluate the dye removal efficiency and reusability of MC with other adsorbents.

(vii) To elucidate the mechanisms involved in the adsorption processes of CV, MB, BG, and MG onto MC.

2. Experimental

2.1. Materials

Ethyl-2-(2-aminothiazol-4-yl)acetate (98%) and NaOH (99,99%) were purchased from Sigma-Aldrich Co.; the microcrystalline cellulose powder (MCC) was purchased from Alfa Aeser Co.; and phosphorous oxychloride ($POCl_3$), extra pure dimethylformamide (DMF), crystal violet (CV), brilliant green (BG), methylene blue (MB), malachite green (MG), HNO_3 (65%), HCl (37%), sodium acetate dihydrate, and glacial acetic acid were bought from Merck Co. All of the chemicals and reagents used in this work were of pure analytical reagent grade. Double-distilled water (DDW) was used throughout the experimental work.

2.2. Preparation of the modified cellulose adsorbent

2.2.1. Preparation of chlorodeoxycellulose (cellulose–Cl). One gram of microcrystalline cellulose was suspended in 20 mL of DMF for 1 h and then reacted with 0.5 mL of $POCl_3$ under mechanical stirring for more than 30 min at 90 °C until the color of the solution changed to dark brown due to the release of phosphoric acid. The obtained chlorodeoxycellulose (cellulose–Cl) was filtered and then washed with DMF, DDW, 5% NaOH, DDW again, 5% acetic acid, and finally with DDW till the color of the product returned to white, indicating the removal of all side products. In the end, the collected powder was dried in air for 24 h.[10,16,17]

2.2.1.1 Estimation of the chloro group content. Firstly, a sample of 0.5 g of cellulose–Cl was directly reacted with 5 mL of hydrazine hydrate (HH) without any solvent. The reaction mixture was stirred under heating at 80 °C for 3 h. The product (cellulose–N) obtained was filtered, washed with DDW and then with ethanol and then dried in air.

In the second step, the concentration of the amino group in cellulose–N was estimated using a volumetric method as follows: 40 mL of a 0.05 M HCl solution was added to 0.1 g of cellulose–N and conditioned for 15 h on a vibromatic shaker.

The residual concentration of HCl was estimated through titration against a 0.05 M NaOH solution using phenolphthalein as the indicator. The number of moles of HCl interacting with amine groups and consequently the amine group concentration (mmol g^{-1}) were calculated using the following equation:

$$\text{Concentration of amino groups} = \frac{(M_1 - M_2)}{0.1} \times 40 \text{ (mmole per g of resin)} \quad (1)$$

where M_1 and M_2 are the initial and final concentrations of HCl, respectively.[10,16,17]

2.2.2. Preparation of the modified cellulose composite (MC). The ligand (2-(2-aminothiazol-4-yl)acetohydrazide) was first synthesized by reacting 0.01 mole of ethyl 2-(2-aminothiazol-4-yl)acetate with 0.01 mole of hydrazine hydrate using methanol as a solvent under reflux for 6 h at 80 °C until white crystals were precipitated. The formation of the ligand was confirmed by TLC and by measuring the melting point = 180–183 °C. Scheme 1a shows the reaction steps.[18,19]

Later on, the MC composite was prepared by mixing 0.2 g of 2-(2-aminothiazol-4-yl)acetohydrazide with 0.5 g of cellulose–Cl in DMF as a solvent and refluxing this mixture for 5 h at 80 °C till a yellow powder was precipitated (Scheme 1b).

2.3. Characterization

The elemental analysis of microcrystalline cellulose (MCC), cellulose–Cl, 2-(2-aminothiazol-4-yl)acetohydrazide (ligand) and the MC adsorbent was conducted using a PerkinElmer 2400 CHNS analyzer. A Shimadzu 5800 Fourier transform infrared (FT-IR) spectrometer was utilized for detecting the functional

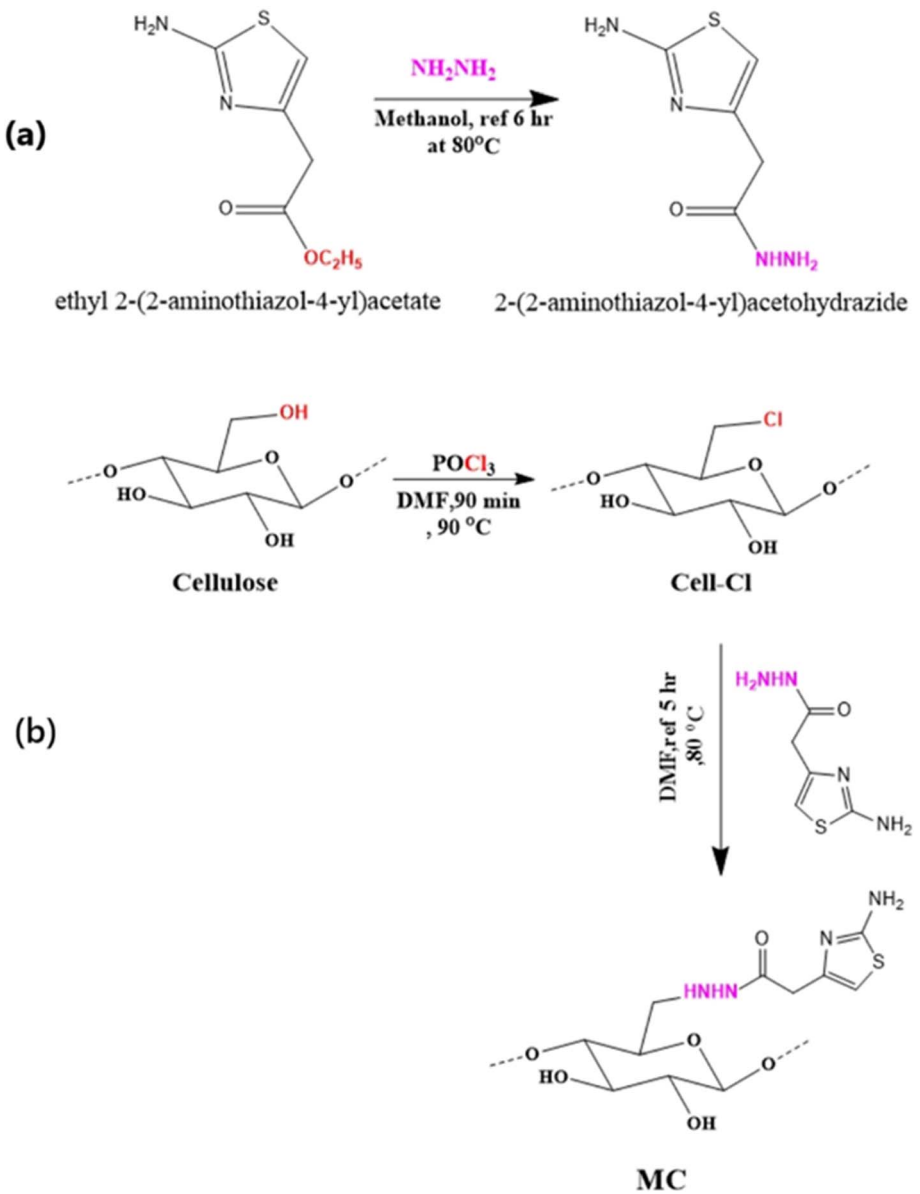

Scheme 1 (a) Synthesis of (a) 2-(2-aminothiazol-4-yl)acetohydrazide. (b) Preparation of the MC composite.

groups in the materials. The surface morphology of pure MCC, cellulose–Cl, and the MC adsorbent before and after the adsorption of the studied dyes were evaluated after sputter-coating with Au ions using a scanning electron microscope (SEM, Quanta FEG-250) and an energy-dispersive X-ray (EDX) microanalysis system at an accelerating voltage of 20 keV at a working distance of 10 μm. ^{1}HNMR spectra were measured in DMSO and trifluoracetic acid (TFA) using the Joel 500 MHZ machine. X-ray diffraction (XRD) patterns were collected using the PANalytical X'Pert PRO diffractometer, covering the 2θ range from 4° to 75°. The Brunauer–Emmett–Teller (BET) equation was applied on the N_2 adsorption isotherms obtained using MICROTRAC (model: BELSORP) (cat. MINI X) (made in Japan) to estimate the specific surface areas of cellulose and the MC adsorbent after the removal of all adsorbed water molecules by drying at 80 °C in a vacuum oven, and the non-localized density functional theory (NLDFT) model was used to calculate the pore size distribution. Both calculations were carried out using BELMASTER (ver. 7) software. The zeta potential was determined using a Malvern instrument as follows: 0.1 g of the MC adsorbent was added to 25 mL of NaOH or HCl solutions with the pH adjusted from 1 to 10. A PerkinElmer 550 spectrophotometer was utilized for determining the concentration of the cationic dyes individually or in binary systems (CV-MB and BG-MG). The highest absorbance values (λ_{max}) for the studied cationic dyes, which include CV, MB, BG, and MG, alongside binary systems (CV + MB) and (BG + MG), were measured across a spectral range from 200 to 900 nm. The λ_{max} for CV, MB, BG, and MG were determined to be 590 nm, 664 nm, 625 nm, and

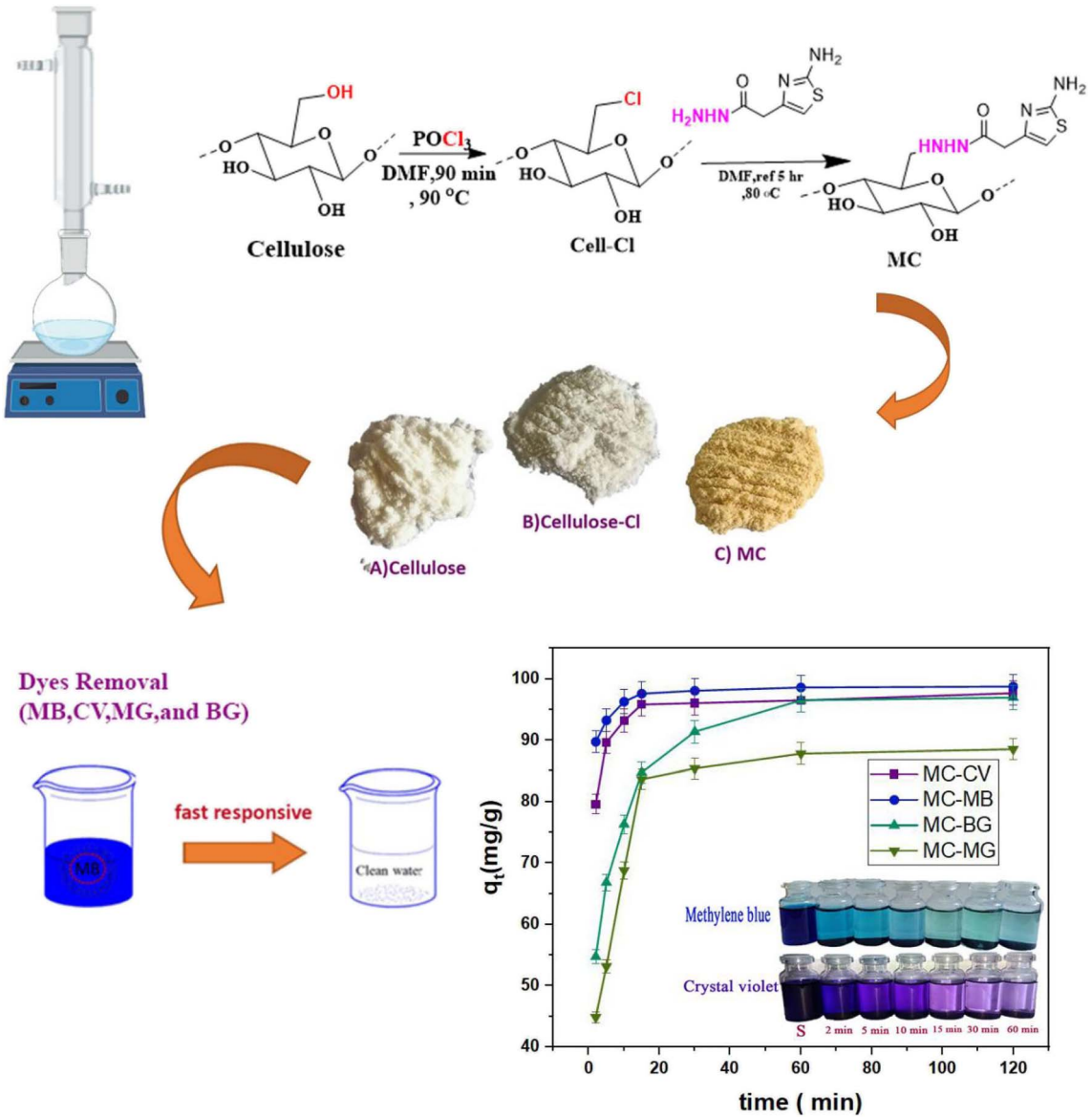

Scheme 2 Synthesis and characterization of the modified cellulose (MC) adsorbent and its use for the adsorption of cationic dyes.

616 nm, respectively. Additionally, binary mixtures such as CV + MB (598 nm and 664 nm) and BG + MG (621 nm) were analyzed.

The synthesis and use of the modified cellulose (MC) adsorbent for the adsorption of cationic dyes are schematically presented in Scheme 2.

2.4. Adsorption tests

The dye adsorption experiments were conducted in the batch mode using 12.5 mL stoppered bottles, each containing 10 mL of the cationic dye solution and a definite amount of the MC adsorbent. The bottles were then agitated at 150 rpm on a thermostatic shaker set to a constant temperature. Once equilibrium was reached, the solutions were centrifuged at 3000 rpm. The supernatant containing the residual cationic dyes was analysed at the specific λ_{max} for each dye. In the case of binary dye systems, the dyes were combined in a 1 : 1 ratio of CV and MB or BG and MG solutions. Various parameters were examined, including contact time (ranging from 2 to 120 minutes), temperature (308–328 K), MC adsorbent dose (0.25–2 g L^{-1}), pH (ranging from 2 to 12), ionic strength, and initial concentration of the studied dyes (25–600 mg L^{-1}). The adsorption capacity (q_e) and removal (R%) were estimated from eqn (2) and (3), respectively.[20]

$$q_e = \frac{(C_i - C_e)V}{m} \quad (2)$$

$$R(\%) = \frac{(C_i - C_e)}{C_i} \times 100 \quad (3)$$

Herein, C_i and C_e (mg L^{-1}) are the initial dye concentration and the equilibrium concentration after adsorption, respectively. V (L) is the volume of the dye solution, and m (g) is the mass of the MC adsorbent. Each measurement's reading was an average of three replicates.

For the adsorption of binary systems, 1 g L^{-1} of the MC adsorbent was added to the binary system solutions, containing 50 ppm of each dye, at a pH of 6 for (BG + MG) and pH of 10 for (CV + MB). The mixture was then agitated at 150 rpm for different time frames. The equilibrium concentration of the adsorbates was derived from UV-Vis data. The efficiency of cationic adsorbate adsorption was determined using eqn (2).

2.5. Desorption and regeneration experiments

The regeneration of the MC adsorbent was examined through 5 repeated cycles of adsorption–desorption by the batch method. In each test, 1 g L^{-1} of the MC adsorbent was shaken with 100 ppm of CV, MB, BG and MG. Then, the adsorbent was filtered and eluted using different eluents including ethanol, HCl (0.2 M), or a 1 : 1 mixture of ethanol and HCl (0.2 mol L^{-1}). This procedure was repeated for 5 cycles consecutively. The desorption efficiency (D, %) was calculated using the formula:

$$D\% = \frac{\text{amount of desorbed dye } (\text{mg L}^{-1})}{\text{amount of adsorbed dye on MC } (\text{mg L}^{-1})} \times 100 \quad (4)$$

3. Results and discussion

3.1. Materials' design and physicochemical studies

3.1.1. Material design. Because the modification of cellulose occurred at the Cl atom, it was necessary to calculate the Cl content in cellulose–Cl. This was carried out by substituting Cl with the NH_2 group and then using the volumetric method to estimate the NH_2 content, which is equivalent to the Cl content. The analysis revealed that cellulose–Cl contained 3.34 mmol Cl per g. The water solubility of the prepared MC was investigated as well to avoid any leaching during the application of MC in the adsorption process. There was no noted decrease in the overall mass of MC, indicating the water insolubility of the prepared MC. Additionally, the MC adsorbent was tested on two types of bacteria, gram +ve bacterium (*S. aureus*) and gram −ve bacterium (*E. coli*). The results confirmed that the prepared MC adsorbent had no antibacterial activity against the two tested bacteria in the water medium.

3.1.2. Elemental analysis. The results of the elemental analysis of 2-(2-aminothiazol-4-yl)acetohydrazide (ligand), cellulose, cellulose–Cl and the MC adsorbent are shown in Table 1S. The successful preparation of the ligand was confirmed by comparing the measured and calculated values. The MC adsorbent had nitrogen (10.4%) and sulphur (5.98%) elements, proving the effective modification of cellulose–Cl with the ligand. It was estimated that the inserted ligand units had a concentration of nearly 3.2 mmol g^{-1}.

3.1.3. BET analysis. The adsorption affinity of a material is directly linked to its texture. The quantity of nitrogen gas adsorbed at 77 K on the prepared MC adsorbent at various relative equilibrium pressures (P/P_0) was measured and plotted in Fig. 1Sa and b. Both cellulose and the MC adsorbent exhibit type III nitrogen gas physisorption isotherms, as categorized by the IUPAC.[21] This isotherm type is characterized by a weak sorption between the adsorbent and adsorbate, lacking a distinct monolayer formation due to the absence of point B. As a result, adsorbed molecules form clusters on the most suitable sites of the adsorbate surface. Both isotherms show H3-type hysteresis loops, indicating that these adsorbents have a macroporous structure.[21] The BET specific surface area was calculated based on the collected N_2 adsorption isotherms. The surface area of cellulose is 0.15 m^2 g^{-1}, with a total pore volume of 0.0079 cm^3 g^{-1} and an average pore diameter of 210.6 nm. In comparison, the MC adsorbent shows values of 0.49 m^2 g^{-1}, 0.0088 cm^3 g^{-1}, and 71.04 nm for these respective parameters. According to Fig. 1Sc and d, the samples can be classified as macroporous, according to the International Union of Pure and Applied Chemistry (IUPAC),[22] which classifies pores as micropores (<2 nm), mesopores (2–50 nm) and macropores (>50 nm). It can be deduced that the higher total pore volume of the MC adsorbent occurs due to the chlorination step, while the decrement in the average pore diameter of the MC adsorbent is caused by the functionalization with the ligand, which fills these pores. Therefore, the chlorination step causes the formation of a higher number of narrow pores. However, these pores are still accessible by the studied dyes because the mean

pore diameter of the MC adsorbent (71.04 nm) is greater than the diameter of the studied dyes (5–25 nm). These characteristics suggest the coordination of the studied dyes with the functional groups on the MC adsorbent internal and external surfaces as the primary mechanism of the adsorption process.

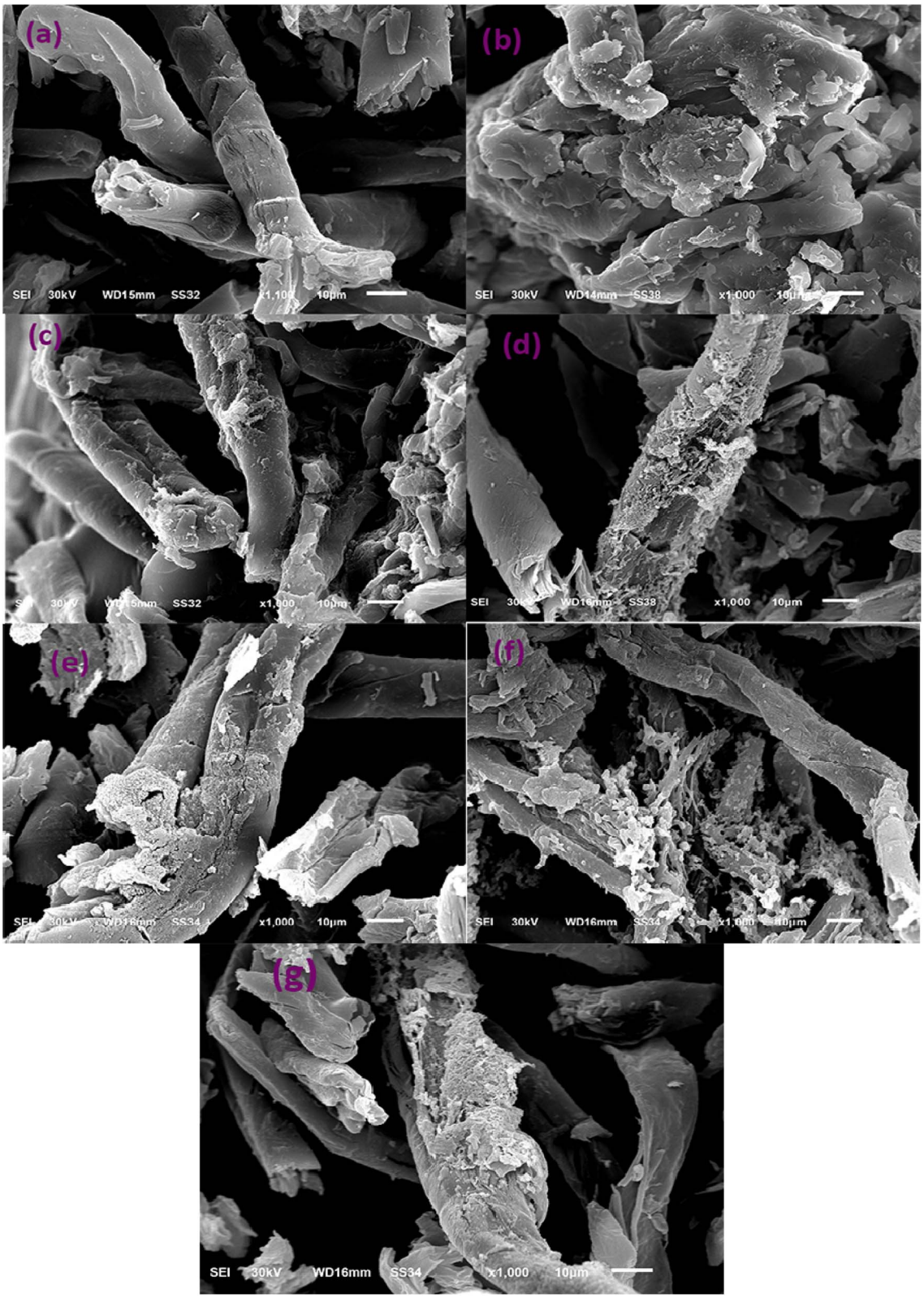

Fig. 1 SEM photographs of (a) microcrystalline cellulose, (b) cellulose–Cl, (c) MC, (d) MC-MB, (e) MC-CV, (f) MC-BG, and (g) MC-MG.

3.2. Characterization

3.2.1. SEM/EDX. SEM analysis (Fig. 1) was used to detect the surface morphology of the materials. While microcrystalline cellulose has irregular microfibers, cellulose–Cl has a coarser surface with several small pores inside compared to that of native cellulose, as shown in Fig. 1b. The surface morphology of the MC adsorbent has not changed significantly relative to that of cellulose–Cl (Fig. 1c), indicating that the ordered structure of the cellulose powder is maintained after the addition of ligand moieties. The SEM morphology of the MC adsorbent after dye adsorption is shown in Fig. 1d–g.

The EDX measurements were conducted on the captured SEM images. Cellulose–Cl displays clear signals at 0.1 and 2.35 keV (Fig. 2b), linked to chloride, which are not seen in cellulose (Fig. 2a). Meanwhile, the MC adsorbent (Fig. 2c) shows distinct signals at 0.2 and 2.2 keV, corresponding to nitrogen and sulphur elements, respectively, with the disappearance of the chloride signal compared to cellulose–Cl. This further confirms the success of the modification step.

3.2.2. XRD. The XRD method was utilized to assess the crystallinity of cellulose after modification. The X-ray diffractograms of cellulose, cellulose–Cl, and the MC adsorbent are presented in Fig. 3. A reduction in the crystallinity of cellulose was observed after chlorination.[23,24]

The crystallinity of the samples was calculated from diffraction intensity data using the empirical method (eqn (5)) for native cellulose.[25]

$$\text{Cr.I}\ (\%) = \frac{I_{002} - I_{\text{am}}}{I_{002}} \quad (5)$$

where Cr.I is the crystallinity index, I_{002} is the maximum intensity (in arbitrary units) of the diffraction from the 0 0 2 plane at $2\theta = 22.6°$, and I_{am} is the intensity of the background scatter measured at $2\theta = 19.5°$. The XRD diffractogram, at $2\theta = 22.6°$, shows that the intenisty decreased in the order from cellulose then cellulose–Cl and then MC adsorbent. On the other hand, the intensity, at $2\theta = 19.5°$, descreased in the following order: cellulose then cellulose–Cl and then MC

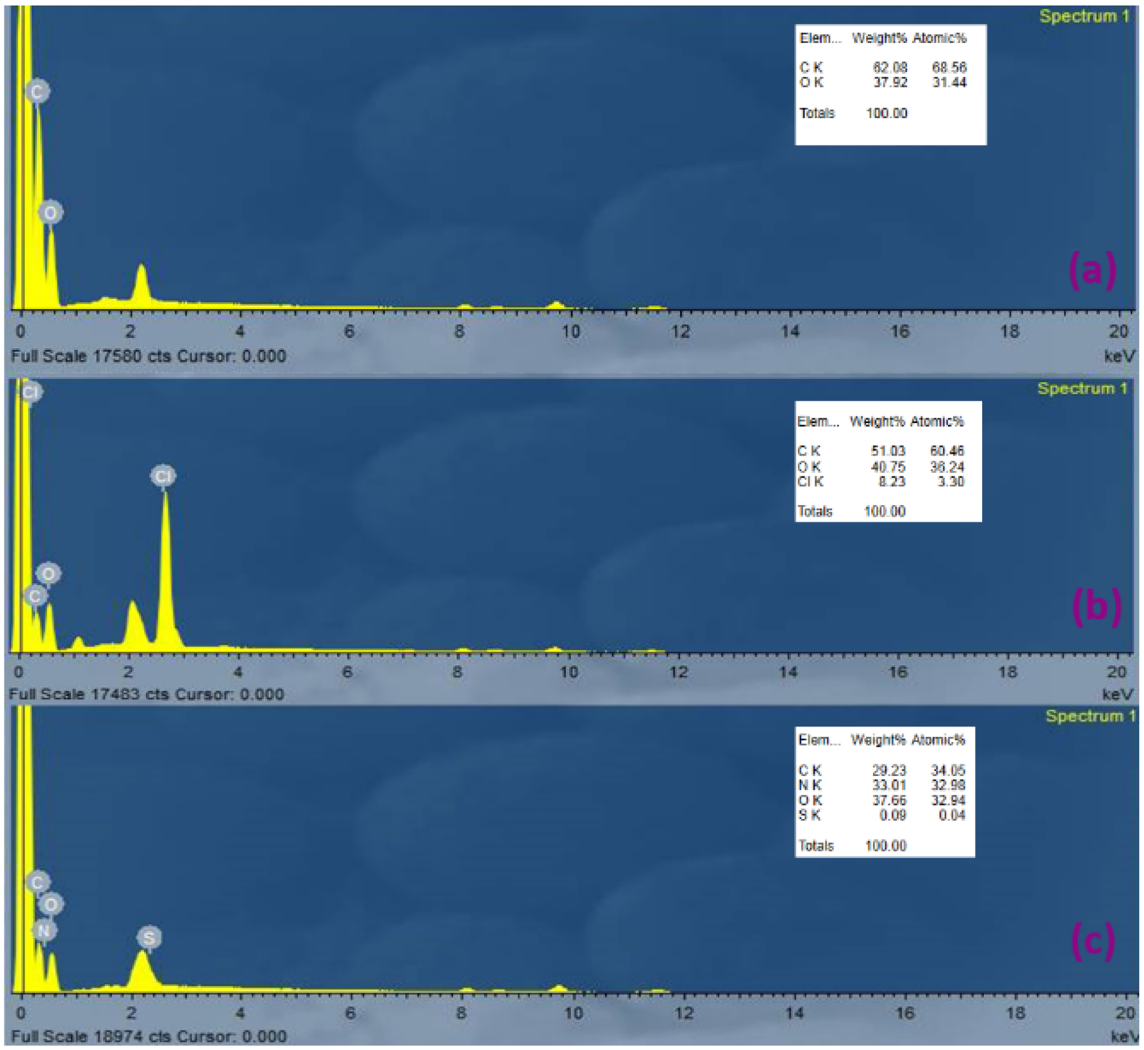

Fig. 2 EDX spectra of (a) microcrystalline cellulose, (b) cellulose–Cl, and (c) modified cellulose (MC).

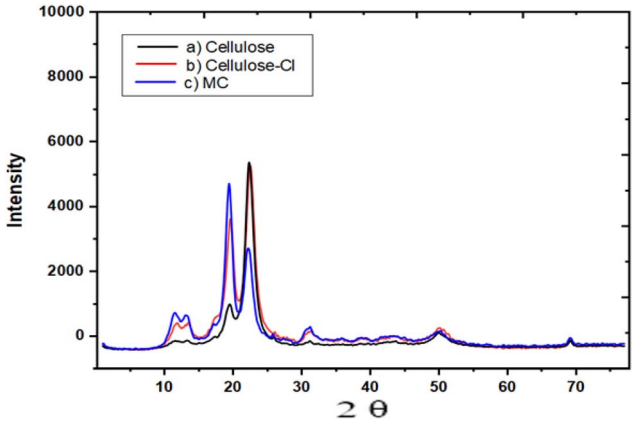

Fig. 3 XRD patterns of (a) microcrystalline cellulose, (b) cellulose–Cl, and (c) the MC adsorbent.

adsorbent. This confirms the decrease in crystallinity which was measured to be 74%, 28% and −62% for cellulose, cellulose–Cl and MC, respectively. The negative value of crystallinity of MC is due to amorphousness.

3.2.3. Infrared spectra. The subsequent steps for the synthesis of the MC adsorbent were investigated using FT-IR spectra, and the findings are presented in Fig. 4.

For microcrystalline cellulose (Fig. 4a), the infrared spectrum shows peaks at 1070–1150 cm^{-1} that may be attributed to C–O stretching vibrations, while those at 1250–1420 cm^{-1} and 3200–3500 cm^{-1} can be attributed to OH bending and stretching vibrations, respectively.[26,27]

For cellulose–Cl (Fig. 4b), the apparent peak around 714 cm^{-1} corresponds to the carbon–chlorine stretching vibration, confirming the presence of chlorine in the structure.[9]

The infrared spectrum of the MC adsorbent (Fig. 4c) exhibits new peaks at 1280 cm^{-1} and 840 cm^{-1}, which may be due to the S–C group of the ligand in the MC adsorbent. In addition, the peaks detected at ~1650 cm^{-1} and 1550 cm^{-1} may be attributed to the stretching vibrations of the O=C group and bending vibrations of the N–H bond, respectively.[28]

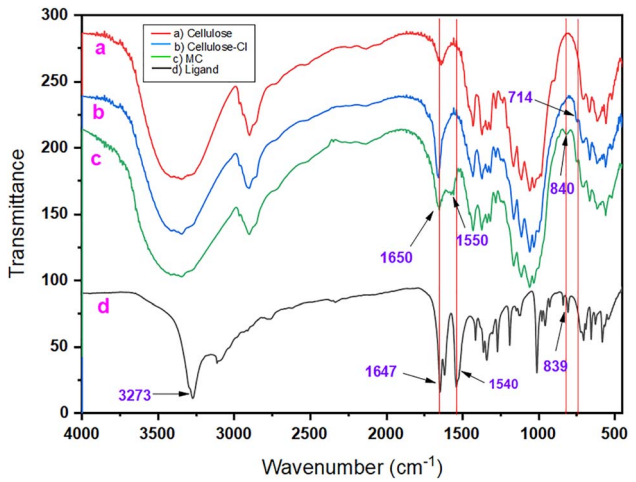

Fig. 4 FTIR spectra of (a) microcrystalline cellulose, (b) cellulose–Cl, (c) MC and (d) the ligand.

The infrared spectrum of the ligand (Fig. 4d) exhibits new relative peaks at 1280 cm^{-1} and 839 cm^{-1} that may be attributed to the S–C group of the ligand. In addition, the peaks detected at ~1647 cm^{-1} and 1540 cm^{-1} may be assigned to the stretching vibrations of O=C and C=N groups and bending vibrations of the N–H bond, respectively. The peaks detected at ~3273 cm^{-1} are due to the stretching vibrations of NH_2.[18,19]

3.2.4. ^{1}H NMR. The most frequent analytical tools used to study the structure of cellulose are solid- and liquid-phase nuclear magnetic resonance (NMR). In this work, a DMSO/trifluoracetic acid mixture was used to dissolve the prepared substances for ^{1}H NMR analysis. ^{1}H NMR confirms the structure of cellulose, cellulose–Cl and the MC adsorbent, as presented in Fig. 5. Specifically, the ^{1}H NMR of cellulose presented in Fig. 5a shows a peak at 1.1 ppm, which is related to the proton present on C_3, C_4, or C_5. By contrast, the peaks appearing at 1.45 ppm and 0.75 ppm are related to the 2H of C_6 and the H of C_2, respectively. Fig. 5b presents the ^{1}H NMR trace of cellulose–Cl, showing shifted peaks (1) at 1.05 ppm related to the proton present on C_3, C_4, or C_5 and (2) at 1.25 ppm and 0.8 ppm related to the 2H of C_6 and the H of C_2, respectively. The ^{1}H NMR of the MC adsorbent (Fig. 5c) shows peaks at 7.9 ppm, 7.19 ppm, 7.05 ppm, 6.95 ppm, 2.8 ppm, and 2.7 ppm, which are attributed to $(NH)_a$, $(NH)_b$, NH_2, CH and CH_2 of the ligand, respectively.[29–31]

3.3. Adsorption studies

3.3.1. Zeta potential and the effect of pH. The zeta potential of the MC adsorbent in relation to pH values is illustrated in Fig. 6a. Clearly, the zeta potential of the MC adsorbent is greatly influenced by the solution's pH level. At very low pH levels (below 2.3), the MC adsorbent is positively charged due to the protonation of ketone, enol forms, and amine groups (*i.e.*, MC–C–OH_2^+ and MC–NH_3^+). As the pH increases, the zeta potential decreases and becomes negative because of the deprotonation of ketone and enol form amines (*i.e.*, MC–C–O^- and MC–NH_2). The zeta potential is 0 at a pH of approximately 2.3–2.4, indicating that the isoelectric point (IEP) of the MC adsorbent falls within this pH range, which confers a negative zeta potential, leading to a negative charge on the surface of the MC adsorbent. Consequently, the enhanced selectivity and efficiency of the MC adsorbent in removing cationic dyes like MB, CV, MG, and BG can be partly attributed to the electrostatic interactions between the positively charged dye molecules and the negatively charged surface of the MC adsorbent.

The adsorption performance of the MC adsorbent for the studied dyes at different pH values is shown in Fig. 6b. As can be noticed, when the other conditions are kept unchanged, the adsorption capacities of the MC adsorbent for the studied dyes are pH-dependent.

The surface sites of the MC adsorbent are protonated at a pH lower than the isoelectric point (2.3) and will be positively charged, and they will be deprotonated at a pH higher than the isoelectric point (2.3) and will be negatively charged. At a pH

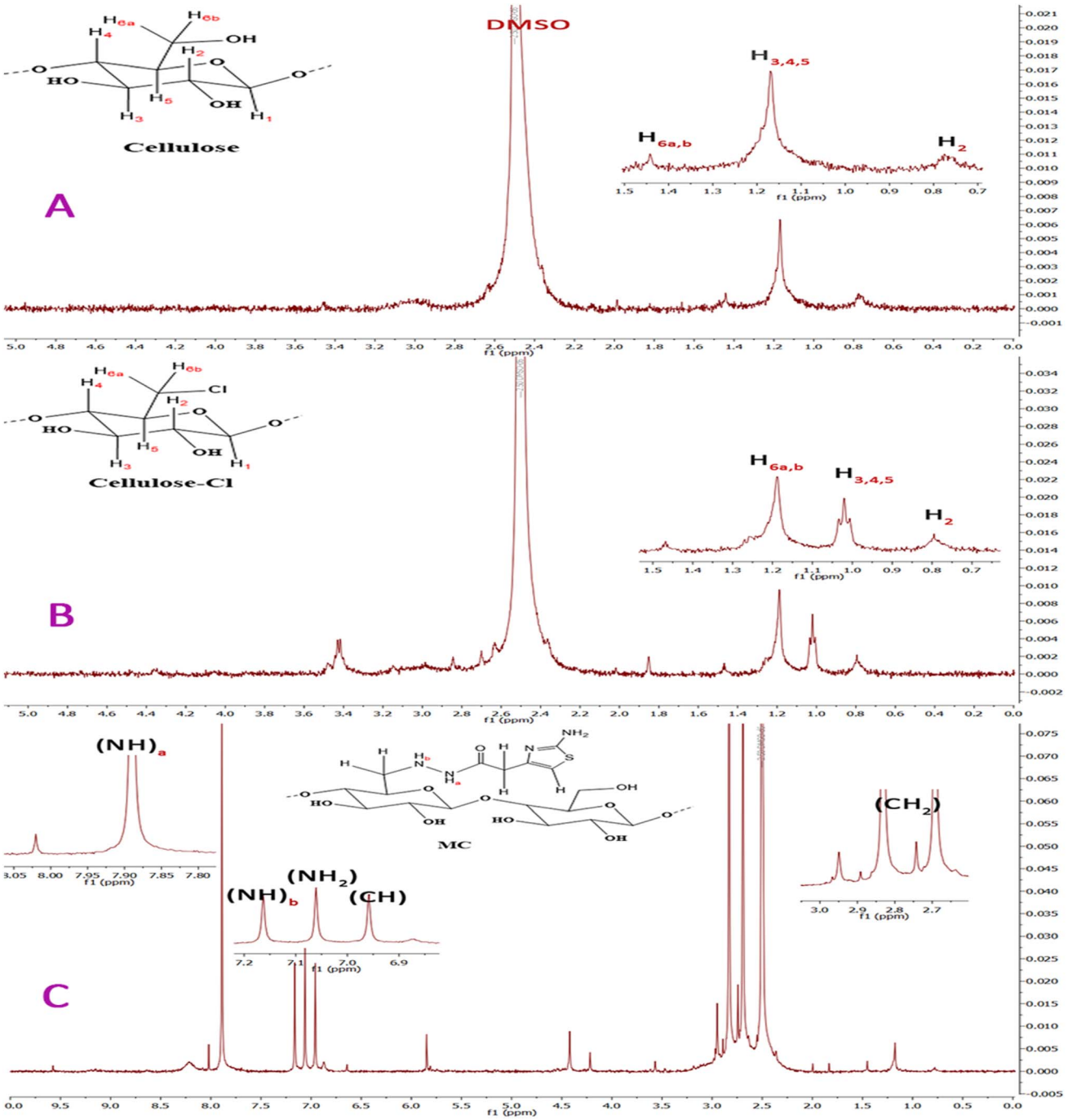

Fig. 5 ^{1}H NMR spectra of (a) MCC, (b) cellulose–Cl, and (c) the MC adsorbent.

lower than the isoelectric point (2.3), the adsorption efficiency (q_e) of the MC adsorbent is low, and this may be attributed to the competition between the studied cationic dyes and H^+ ions for the available surface sites at this pH. This competition decreases after increasing the pH, resulting in better adsorption. Therefore, the optimum pH can be considered to be 6 for BG and MG dye adsorption and 10 for the adsorption of CV and MB dyes.

3.3.2. Effect of the MC dose. Fig. 2S shows the effect of the MC amount on the adsorption of CV, MB, BG and MG dyes. Apparently, the adsorption efficiency (q_e) increases rapidly from 0.25 to 1 g L^{-1} and then decreases from 1 to 2 g L^{-1} with an increase in the MC amount from 0.25 to 2 g L^{-1}. This is logical as more adsorption sites become available with increasing MC dose. When the MC amount increases further, the studied dyes are basically adsorbed completely. Therefore, increasing the MC amount does not lead to a higher adsorption efficiency (q_e). Accordingly, 1 g L^{-1} of MC adsorbent was decided to be the optimal dose.

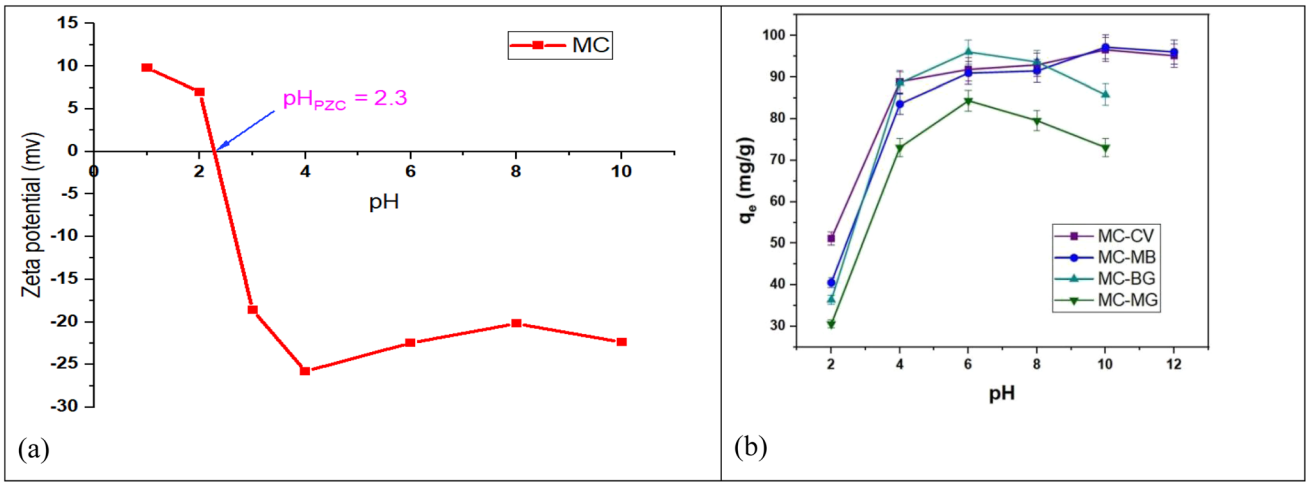

Fig. 6 (a) Zeta potential of MC *versus* pH values and (b) effect of pH on the adsorption performance of MC. Studied dyes (100 mg L^{-1}), sorbent (1 g L^{-1}), pH = 6 for BG and MG and pH = 10 for CV and MB at 308 K.

3.3.3 Effect of the initial dye concentration. The study examined how different initial concentrations of cationic dyes (CV, MB, BG, and MG) affected their adsorption onto the surface of the MC adsorbent, with values ranging from 25 to 600 ppm, while keeping the other parameters fixed. The findings shown in Fig. 3S reveal an increase in the adsorption capacity for CV, MB, BG, and MG, increasing from 25 mg g^{-1} to 170 mg g^{-1}, 25 mg g^{-1} to 172.3 mg g^{-1}, 25 mg g^{-1} to 185.4 mg g^{-1}, and 25

Table 1 Adsorption isotherm fitting parameters

	Parameters				
Isotherm models	System	MC-MB	MC-CV	MC-BG	MC-MG
Langmuir	K_F	67.95 ± 10.488	64.12 ± 9.860	57.88 ± 7.063	45.78 ± 5.763
	n	5.95 ± 1.13	5.72 ± 1.03	4.89 ± 0.59	9.37 ± 2.25
	R^2	0.895	0.907	0.866	0.837
	Adj. R^2	0.875	0.889	0.839	0.805
	χ^2	423	364	619.4	93.3
	SSE	2118.78	1820.76	3097.12	466.54
	MSE	302.68	260.1	442.44	66.64
Freundlich	K_F	67.95 ± 10.488	64.12 ± 9.860	57.88 ± 7.063	45.78 ± 5.763
	n	5.95 ± 1.13	5.72 ± 1.03	4.89 ± 0.59	9.37 ± 2.25
	R^2	0.895	0.907	0.866	0.837
	Adj. R^2	0.875	0.889	0.839	0.805
	χ^2	423	364	619.4	93.3
	SSE	2118.78	1820.76	3097.12	466.54
	MSE	302.68	260.1	442.44	66.64
	q_m (mg g^{-1})	147.06 ± 11.03	143.01 ± 12.07	145.28 ± 15.82	79.22 ± 2.018
Dubinin–Radushkevich	K_{DR}	0.973 ± 0.36	0.919 ± 0.38	0.893 ± 0.48	0.471 ± 0.06
	E	0.717	0.738	0.748	1.03
	R^2	0.859	0.823	0.733	0.964
	Adj. R^2	0.831	0.788	0.680	0.957
	χ^2	570.37	698.51	1234.57	20.49
	SSE	2851.87	3492	6172.8	102.47
	MSE	407.41	498.85	881.82	14.63
Temkin	K_T	23.93 ± 11.937	21.42 ± 11.045	12.69 ± 4.743	692.07 ± 1122
	b	0.0503 ± 0.004	0.0511 ± 0.004	0.0461 ± 0.003	0.1455 ± 0.023
	R^2	0.969	0.967	0.980	0.887
	Adj. R^2	0.963	0.961	0.976	0.865
	χ^2	123.3	128.8	92.15	64.97
	SSE	616.8	644.04	460.74	324.85
	MSE	88.11	92.00	65.82	46.41

mg g^{-1} to 84.5 mg g^{-1}, respectively, when using 1 g L^{-1} of the MC adsorbent.

Adsorption isotherms give valuable information about how dye molecules move from water to the surface of adsorbents while keeping the pH and temperature constant. To explain the relationship between dye molecules and the surface of the adsorbent created, several mathematical models can be utilized (Table 2S). These models help in determining the design needed for effectively applying the adsorption process in practice. Consequently, as illustrated in Fig. 4S, different adsorption models[32] were applied to the experimental data through non-linear curve fitting. A summary of the parameters obtained is presented in Table 1.

To assess the accuracy of kinetic and isotherm models, the researchers utilized various error functions. These functions aimed to minimize the discrepancy between theoretical predictions and experimental results. The performance evaluation of kinetic models involved several statistical metrics, including R^2, adjusted R^2, chi-square statistic (χ^2), sum of squares error (SSE), and mean square error (MSE), which are presented in eqn (6)–(10),[33] respectively.

$$R^2 = \frac{\sum (q_{mean} - q_{cal})^2}{\sum (q_{cal} - q_{mean})^2 + \sum (q_{cal} - q_{exp})^2} \quad (6)$$

$$\text{Adj. } R^2 = 1 - (1 - R^2)\frac{(N_{exp} - 1)}{(N_{exp} - N_{para} - 1)} \quad (7)$$

$$x^2 = \sum \frac{(q_{exp} - q_{cal})^2}{(q_{cal})^2} \quad (8)$$

$$SSE = \sum (q_{exp} - q_{cal})^2 \quad (9)$$

$$MSE = \frac{1}{N_{exp}} \sum (q_{exp} - q_{cal})^2 \quad (10)$$

Table 1 displays the calculated parameter values for various adsorption isotherm models. The best isotherm model is chosen according to the higher correlation coefficient (R^2) and the lower error functions in comparison to other models.

In order to explore the energetic characteristics, the Temkin isotherm equation was used to fit the experimental data of the adsorption isotherm. The Temkin isotherms are based on the assumption that the adsorption process is defined by a consistent distribution of binding energies. According to the data presented in Table 1, the adsorption heat for all molecules within the layer exhibited a linear decrease as coverage expanded. The dye (CV, MB, and BG) adsorption isotherm for MC aligns well with the Temkin isotherm model (Fig. 4S), as indicated by its high correlation coefficient (R^2) and lower error functions compared to other models (refer to Table 1). In contrast, the Freundlich fitting line was less accurate compared to the experimental data points. The calculated separation factor (R_L) for the adsorption of CV, MB, BG and MG falls within the range from 0 to 1. This suggests that the adsorption process is favorable, which aligns with the findings of R_L. This is due to the better fitting of the correlations in the Temkin isotherm adsorption model. Meanwhile, the adsorption isotherm of MG on MC aligns well with the Langmuir isotherm model (Fig. 4S),

Table 2 Kinetic parameters for the adsorption of the studied dyes onto the MC adsorbent

	Parameters				
Models	System	MC-MB	MC-CV	MC-BG	MC-MG
Pseudo-first-order	K_1 (min^{-1})	0.513 ± 0.069	0.469 ± 0.083	0.168 ± 0.026	0.188 ± 0.022
	q_e (mg g^{-1})	97.3 ± 0.47	96.27 ± 0.67	95.12 ± 0.02	87.53 ± 0.88
	R^2	0.999	0.999	0.997	0.999
	Adj. R^2	0.998	0.998	0.997	0.998
	χ^2	1.2	1.88	6.32	2.31
	SSE	8.32	9.426	31.59	11.57
	MSE	1.18	1.346	4.51	1.65
Pseudo-second-order	K_2 (g mg^{-1} min^{-1})	0.0476 ± 0.0047	0.0224 ± 0.0009	0.0054 ± 0.0009	0.0041 ± 0.0009
	q_e (mg g^{-1})	98.67 ± 0.36	97.82 ± 0.27	96.72 ± 2.36	91.65 ± 3.28
	R^2	0.961	0.994	0.952	0.935
	Adj. R^2	0.953	0.993	0.942	0.923
	χ^2	0.527	0.27	14.8	24.85
	SSE	2.636	1.398	74.03	124.27
	MSE	0.376	0.199	10.57	17.75
Elovich	a_e	$2.23 \times 10^{18} \pm 1.89 \times 10^{19}$	$4.04 \times 10^{9} \pm 2.22 \times 10^{10}$	1102.9 ± 792.606	368.72 ± 377.062
	q_e (mg g^{-1})	0.460 ± 0.090	0.254 ± 0.061	0.091 ± 0.010	0.085 ± 0.016
	R^2	0.838	0.773	0.944	0.856
	Adj. R^2	0.806	0.728	0.933	0.828
	χ^2	2.199	10.95	16.97	55.20
	SSE	10.99	54.79	84.87	277.20
	MSE	1.57	7.82	12.12	39.6

as indicated by its high correlation coefficient R^2 and lower error functions compared to other models.

The Dubinin–Radushkevich (D–R) isotherm model was utilized to estimate the adsorption energy (E) and determine the nature of the adsorption (Table 1). The adsorption energy (E) value provides details about the physical or chemical nature of the adsorption process. When E is less than 8 kJ mol^{-1}, physisorption can explain the type of adsorption; when E is greater than 8 kJ mol^{-1}, ion-exchange or chemical adsorption controls it.[34–36] The D–R isotherm fitting curve is displayed in Fig. 4S, and Table 1 provides the determined parameters. The calculated adsorption energy (E < 8 kJ mol^{-1}) indicates that physisorption can account for the type of adsorption for the studied dyes onto MC. This means that adsorption is reversible and is characterized by the formation of weak physical attraction forces between adsorbate molecules and the solid surface, such as hydrogen bonds, electrostatic attraction, and van der Waals forces.

3.3.4. Effect of the contact time and adsorption kinetics. The contact time of CV, MB, BG, and MG with the MC adsorbent is a crucial factor. Hence, it was examined at various shaking durations by using a 1 g L^{-1} concentration of the MC adsorbent in pH-adjusted solutions at a temperature of 308 K, with pH 6 for 100 mg L^{-1} BG and MG and pH 10 for 100 mg L^{-1} CV and MB. Fig. 5S illustrates how the shaking time affects the adsorption of the dyes onto MC. It is evident that the initial adsorption occurs quickly, followed by slower removal that gradually reaches a state of equilibrium. Specifically, approximately 97 mg g^{-1} (97%) of MB, around 96 mg g^{-1} (96%) of CV, nearly 96 mg g^{-1} (96%) of BG, and about 87 mg g^{-1} (87%) of MG are eliminated within the first 2 minutes of contact. The quick adsorption at the beginning can be explained by the higher concentration gradient and a larger number of available sites for adsorption. The highest uptake capacity is reached within 15 minutes for MB and CV and within 60 minutes for BG and MG. During the analysis of the experimental data collected, three

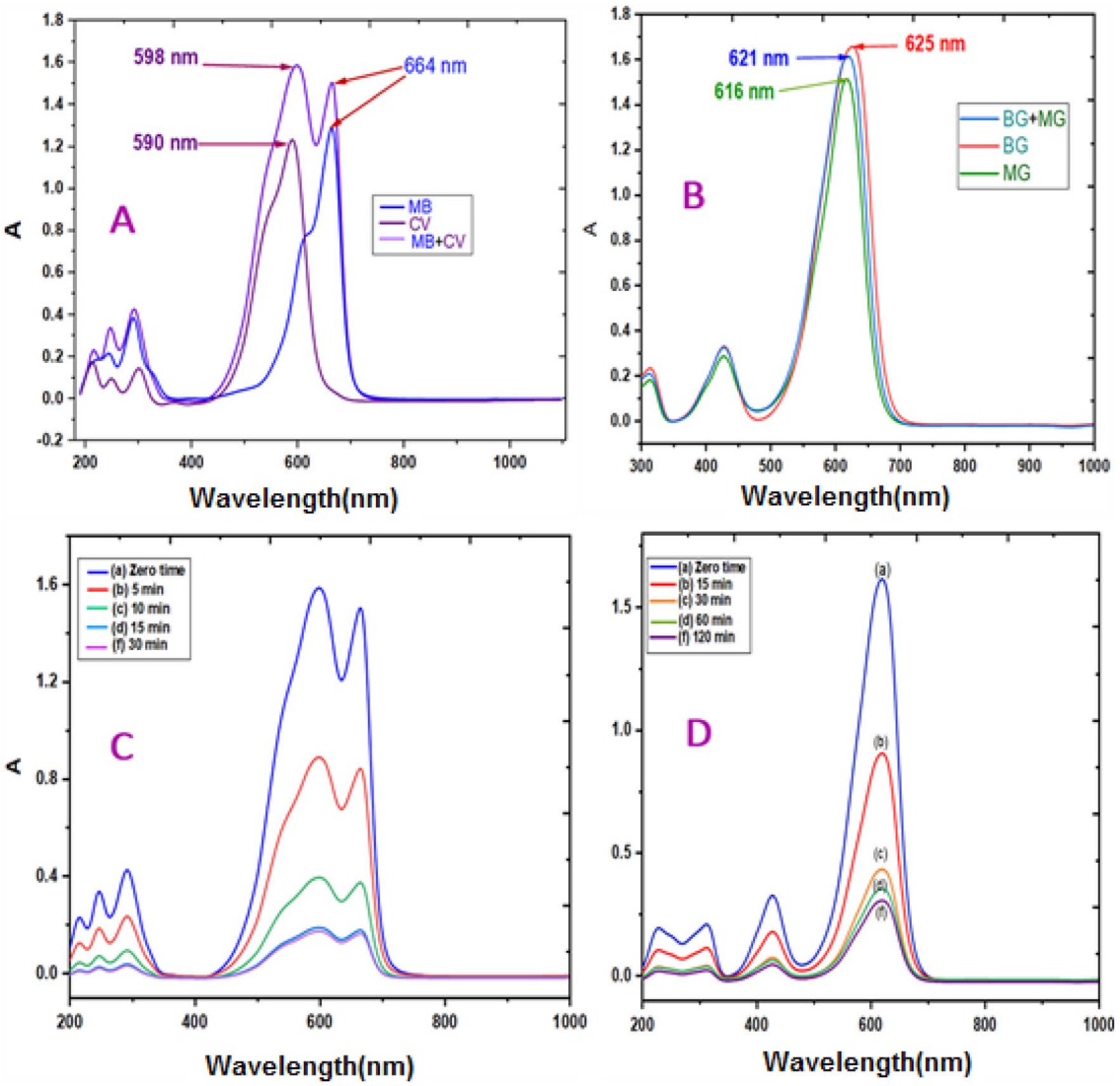

Fig. 7 UV spectra of (A) MB, CV and MB + CV and (B) BG, MG and BG + MG; (C) effect of time on the absorbance of the MB + CV mix on MC; and (D) effect of time on the absorbance of (BG + MG) on MC.

kinetic models were applied: pseudo-first-order, pseudo-second-order, and Elovich (Table 2S). These models are fitted non-linearly, as seen in Fig. 6S. A summary of the equations for these models, along with their extracted parameters, is given in Table 2. To identify which kinetic model best fitted the experimental results, the correlation coefficient (R^2) and various error functions were utilized. The pseudo-first-order model best fitted the adsorption of MG and BG due to the higher R^2 values and lower error functions ((χ^2), (SSE), and (MSE)) compared to those of the pseudo-second-order model. Meanwhile, the pseudo-second-order model best fitted the adsorption of MB and CV due to the higher R^2 values and lower error functions ((χ^2), (SSE), and (MSE)) compared to those of the pseudo-first-order model. Therefore, the pseudo-first-order model is the best fit for the adsorption of MG and BG onto MC, and the pseudo-second-order model is the best fit for the adsorption of MB and CV onto MC. The order of the rate constants for the dyes adsorbed onto the MC adsorbent is determined to be MB > CV > BG > MG, aligning well with the experimental findings.

3.3.5. Thermodynamic studies. Certain measurements like the standard free energy (ΔG°_{ads}), enthalpy heat (ΔH°_{ads}), and adsorption entropy (ΔS°_{ads}) for the studied dyes adsorbed onto MC adsorbent were calculated in the temperature range from 308 to 328 K.

The thermodynamic reaction rate constant (K_c) and other parameters were calculated as follows:[37]

$$K_c = C_{ad}/C_e \quad (11)$$

where C_{ads} denotes the dye concentration sorbed on the MC adsorbent at equilibrium (mg g^{-1}) and C_e denotes the concentration at equilibrium (mg L^{-1}).

$$\Delta G^{\circ}_{ads} = -RT \ln K_c \quad (12)$$

$$\ln K_c = \left(\Delta S^{\circ}_{ads}/R\right) - \left(\Delta H^{\circ}_{ads}/RT\right) \quad (13)$$

where R is the universal gas constant (8.314 J mol^{-1} K^{-1}). The slope (H°_{ads}/R) and intercept (S°_{ads}/R) of the plot of $\ln K_c$ *vs.* $1/T$ were used to determine the values of H°_{ads} and S°_{ads}, respectively, as shown in Fig. 7S. From the evaluated thermodynamic parameters given in Table 3S, a negative value of ΔG°_{ads} was obtained, demonstrating the spontaneous adsorption of the studied dyes on the MC adsorbent at 308 K. It is noticeable that the adsorption capacity for the dyes declined as the temperature increased, implying stronger interactions between the dyes and the active groups in the MC adsorbent. This is supported by the negative value of ΔH°_{ads}, which means that the process of adsorption is exothermic in nature, and some amount of heat is lost upon the dyes' adsorption. On the contrary, the negative ΔS°_{ads} values indicate that the system becomes more organized and has less randomness after adsorption.

3.3.6. Effect of the ionic strength. Because industrial wastewater contains a lot of various solutes, the ionic strength becomes a crucial factor affecting the provided method's selectivity. Therefore, different ions were added to the studied dyes' solutions (0.1 M NaCl, 0.1 M KCl, 0.1 M $MgCl_2$, 0.1 M $AlCl_3$, and 0.1 M CH_3COONa). Then, the adsorption performance was monitored under the pre-determined optimum conditions. According to the data shown in Table 4S, there is no obvious effect of the ionic strength on the adsorption of dyes.

3.3.7. Removal of CV, MB, BG and MG in a binary system. Because organic pollutants or dyes are found in various forms in real contaminated water, it is crucial to explore the removal potential of MC in the binary dye systems studied. The adsorption studies were conducted at the λ_{max} of each pollutant. Fig. 7 displays the UV results of the binary systems after adsorption by the MC adsorbent. The adsorption equilibrium was achieved after 2 h for the BG + MG system and after 30 minutes for the CV + MB system, indicating that the time for adsorption equilibrium was doubled compared with mono systems because of the increased competition of the two dyes toward the adsorption sites on MC. Upon mixing the dyes, new overlapping peaks emerged in the absorption spectra, as shown in Fig. 7a–d.

3.3.8. Desorption and reusability studies. To examine the reusability of the MC adsorbent, five cycles of adsorption and desorption for individual dyes were performed under the optimized conditions. Various eluents were tested like HCl 0.2 M and ethanol and a mixture of ethanol and 0.2 M HCl in a 1 : 1 ratio. It was determined that a mixture of ethanol and 0.2 M HCl in a 1 : 1 ratio was the most effective eluent, achieving desorption efficiencies of 98.9%, 98.6%, 97.7% and 97.4% for CV, MB, BG, and MG, respectively. In Fig. 8Sa, the impact of different eluents on the desorption of CV, MB, BG, and MG is illustrated, while Fig. 8Sb presents the data from the five repeated cycles of adsorption and desorption for CV, MB, BG, and MG using the 1 : 1 ethanol and 0.2 M HCl mixture as the eluent. After five cycles, the recovery % was measured to be 91.5%, 91.2%, 90.4% and 90.5%, for CV, MB, BG, and MG, respectively. These results indicate that the material maintains consistent performance

Fig. 8 Optical images of (A) cellulose, (B) cellulose–Cl, (C) MC, (D) MC-MB, (E) MC-CV, (F) MC-BG, and (G) MC-MG.

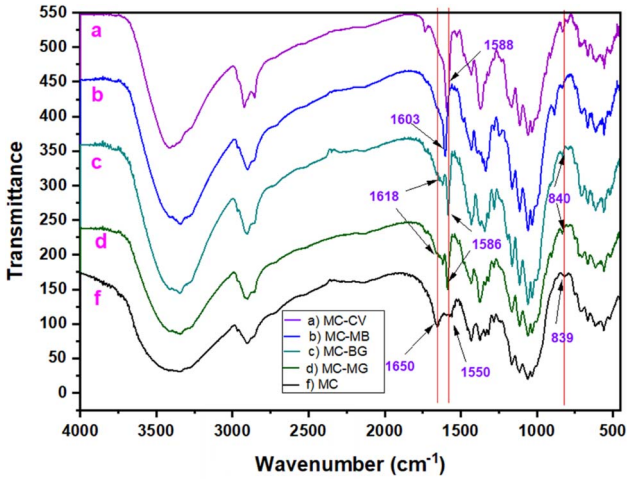

Fig. 9 FTIR spectra of (a) MC, (b) MC-MG, (c) MC-BG, (d) MC-MB, and (e) MC-CV.

over five successive adsorption cycles, achieving an adsorption efficiency of more than 90%. This demonstrates the potential use of the MC adsorbent.

3.3.9. Plausible mechanism of adsorption. The mechanism of adsorption of the studied dyes onto the MC adsorbent can be explained using the FTIR spectra of MC before and after the loading of studied dyes and the results from the D–R model. This will be discussed in the following section.

3.3.9.1 Optical images. Fig. 8a–g displays the optical images of cellulose, cellulose–Cl, and the MC adsorbent before and after dye loading (MC-MB, MC-CV, MC-BG, and MC-MG). The photographs show a clear colour difference between the MC adsorbent before and after dye uptake, which is converted from yellow for the MC adsorbent (Fig. 8c) to dark blue, violet, pale green, and dark green beige for MC-MB, MC-CV, MC-BG, and MC-MG, respectively, as shown in Fig. 8d–g. These findings demonstrate that the studied dyes completely penetrate and adsorb within the MC texture.

3.3.9.2. FTIR spectra of MC before and after the adsorption of dyes. There were important differences observed when comparing the FTIR spectra of MC before the dye adsorption (Fig. 9a) with those after the process (Fig. 9b–e). New peaks emerged in the spectra; specifically, one related to the aromatic alkene C=C at 1520 cm^{-1} for the MC material was observed following the adsorption of the four dyes. The peak near ~3430 cm^{-1} widened after the adsorption of CV, MB, BG, and MG, which could be due to the formation of hydrogen bonds. The peaks detected at ~1650 cm^{-1} and 1550 cm^{-1} may be attributed to the stretching vibrations of the O=C group and the bending vibrations of the N–H bond of the ligand, respectively, which shifted from 1650 cm^{-1} to a lower wavenumber and 1550 cm^{-1} to a higher wavenumber. These shifts confirmed that the studied dyes were adsorbed on MC.

Therefore, there are two expected interactions between the investigated dyes (CV, MB, BG and MG) and the MC adsorbent:

(1) Electrostatic interaction between the $C{=}S^{+}$ positive charge of MB as well as the $C{=}N^{+}$ positive charge of CV, BG and MG and the negative charge on the MC surface ($C{-}O^{-}$).

(2) Hydrogen bonding between the hydroxyl (OH) group of the MC adsorbent (Fig. 10) and the hydrogen atoms of the benzene (C_6H_6) rings found in the studied dyes.

Fig. 10 shows a diagram of the adsorption of MB, CV, BG, and MG cationic dyes on the surface of the MC adsorbent.

3.3.10. Applications. The proposed MC adsorbent was utilized to separate and retrieve CV, MB, BG, and MG dyes from various actual samples. These samples included surface water collected from the intake of the water station in Mansoura, tap water from our laboratory at Mansoura University, and seawater from Damietta City. The results are displayed in Table 3. None of the added dyes were found naturally in any of the samples. The recoveries were measured for the samples in which specific amounts of each dye were added. The recoveries ranged from 97.2% to 100%. These results suggest that the MC sorbent can be effectively used for detecting cationic dyes in real water sources.

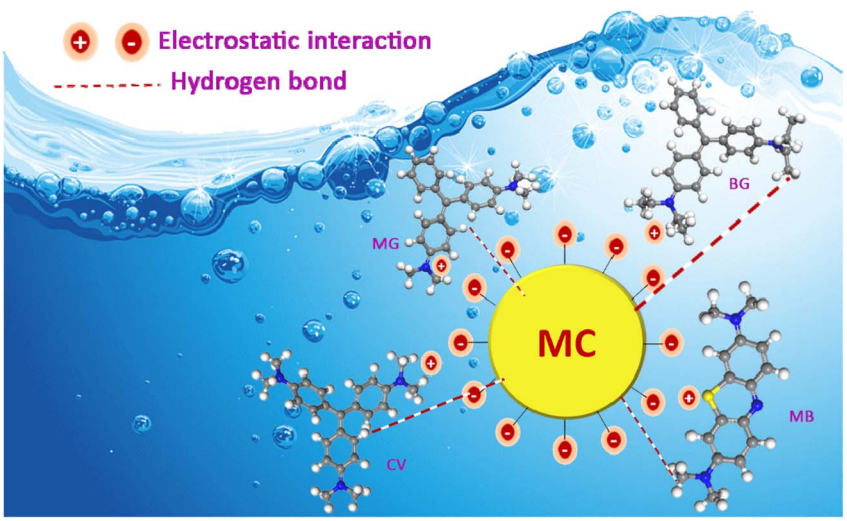

Fig. 10 Schematic of the adsorption of MB, CV, BG, and MG cationic dyes on the surface of the MC adsorbent.

Table 3 Recovery of the cationic dyes CV, MB, BG, and MG from real water samples using the MC adsorbent under ideal conditions ($n = 3$)

Sample	Dyes	Spiked (ppm)	Measured (ppm)	Recovered (ppm)	Recovery (%)	RSD (%)
Tap water	MB	0.00	0.00	0.00	0.00	0.00
		50	0.5	49.5	100	1.23
		100	2.9	97.1	99.84	1.58
	CV	0.00	0.00	0.00	0.00	0.00
		50	0.6	49.4	99.79	1.62
		100	3.5	96.5	99.88	1.57
	BG	0.00	0.00	0.00	0.00	0.00
		50	0.55	49.45	99.89	1.98
		100	6	94	99.4	2.31
	MG	0.00	0.00	0.00	0.00	0.00
		50	0.67	49.33	99.65	1.9
		100	20.9	79.1	98.87	2.25
Sea water	MB	0.00	0.00	0.00	0.00	0.00
		50	1.2	48.8	98.6	2.24
		100	5.1	94.9	97.58	2.05
	CV	0.00	0.00	0.00	0.00	0.00
		50	1.5	48.5	97.97	1.88
		100	7.4	92.6	96	1.97
	BG	0.00	0.00	0.00	0.00	0.00
		50	1.6	48.4	97.77	2.29
		100	8.6	91.4	97.5	2.62
	MG	0.00	0.00	0.00	0.00	0.00
		50	1.8	48.2	97.2	2.09
		100	22.1	77.9	97.37	2.98
Surface water	MB	0.00	0.00	0.00	0.00	0.00
		50	0.6	49.4	99.79	1.76
		100	3	97	99.74	1.49
	CV	0.00	0.00	0.00	0.00	0.00
		50	0.65	49.35	99.7	1.85
		100	3.8	96.2	99.6	1.98
	BG	0.00	0.00	0.00	0.00	0.00
		50	0.6	49.4	99.79	0.98
		100	6.5	93.5	99.64	1.56
	MG	0.00	0.00	0.00	0.00	0.00
		50	0.65	49.35	99.69	1.82
		100	21.2	78.8	98.6	2.12

Table 4 Comparison of the CV, MB, BG and MG sorption capacities of the MC adsorbent with those of the previously reported sorbents

Adsorbate	Adsorbent	Adsorbent dose	Equilibrium time	Sorption capacity (mg g^{-1})	References
MB	Rejected tea	0.50 g/200 mL	180 min	147	38
	Raw algerian kaolin	1.0 g L^{-1}	180 min	52.76	39
	Activated carbon/cellulose composite (ACC)	1.0 g L^{-1}	24 h	103.66	40
	Modified cellulose (MC)	1 g L^{-1}	15 min	173	This work
CV	Charred rice husk (CRH)	25 mg	60 min	62.85	41
	Xanthated rice husk (XRH)	25 mg	60 min	62.85	
	Palm kernel shell-derived biochar	0.5 g	24 h	24.45	42
	Modified cellulose (MC)	1 g L^{-1}	15 min	171.8	This work
BG	Chemically activated date pit carbon	0.06 g	55 min	77.8	43
	Areca nut husk	10 g L^{-1}	120 min	18.21	36
	Modified cellulose (MC)	1 g L^{-1}	60 min	188.6	This work
MG	CMC-*g*-P(AAm)	1 g L^{-1}	240 min	158.1	44
	CMC-*g*-P(AAm)/MMT	1 g L^{-1}	240 min	172.4	
	Modified cellulose (MC)	1 g L^{-1}	60 min	82.17	This work

3.3.11. Performance of the MC adsorbent. The MC adsorbent was effective in separating and removing cationic dyes such as CV, MB, BG, and MG from various water samples with great efficiency. In Table 4, a comparison of MC's performance with other mentioned adsorbents is shown. The highest adsorption efficiencies were observed at an adsorbent dosage of

1 g L^{-1} of MC and an optimal pH of 10 for MB and CV and 6 for BG and MG. Under these optimal conditions, MB and CV were removed from water in just 15 minutes, whereas BG and MG removal required 60 minutes. It was noted that when evaluating different adsorbents for the removal of CV, MB, BG, and MG, factors such as the sorption capacity, the type of adsorbent, the amount of adsorbent used, and the time needed for sorption were important to consider. In conclusion, MC demonstrates superior capacities and efficacy for recovering CV, MB, BG, and MG compared to the other adsorbents listed in Table 4.

4. Conclusion

The study examined the adsorption of dyes onto MC, both individually and in mixtures, under various experimental conditions, such as pH, contact time, initial dye concentration, temperature, and adsorbent dosage, to enhance the adsorption process. The highest adsorption efficiencies were observed at an adsorbent dosage of 1 g L^{-1}, an optimal pH of 10 for MB and CV, and an optimal pH of 6 for BG and MG. Under these optimal conditions, MB and CV were removed from water in just 15 minutes, whereas BG and MG removal required 60 minutes. Kinetic studies, characterized by high R^2 values and lower error functions ((χ^2), (SSE), and (MSE)), indicated that the adsorption of MB and CV dyes conformed well to the pseudo-second-order kinetic model, while BG and MG dye adsorption aligned with the pseudo-first-order kinetic model. Furthermore, the Temkin model best described the sorption isotherm data for MB, CV, and BG, whereas the adsorption of the MG dye was best represented by the Langmuir isotherm model, with maximum adsorption capacities at 308 K of 173.00 mg g^{-1}, 171.80 mg g^{-1}, 188.60 mg g^{-1}, and 82.17 mg g^{-1} for MB, CV, BG, and MG, respectively. The MC could be regenerated successfully for up to four adsorption cycles. Thermodynamic analysis indicated that the adsorption of these cationic dyes onto MC was both spontaneous and exothermic. The prepared MC was also effectively used to remove cationic dyes from actual water samples and synthetic effluents, achieving a recovery rate (R%) higher than 97%. Ultimately, this study demonstrated that the fast-responsive modified cellulose (MC) can be effectively utilized to eliminate cationic dyes from a broad spectrum of real water sources.

Author contributions

Abdelrahman S. El-Zeny: methodology, investigation, writing – original draft. El-Sayed R. H. El-Gharkawy: conceptualization, review, supervision. Tarek A. Gad-Allah: conceptualization, review, supervision. Magda A. Akl: conceptualization, methodology, investigation, writing – original draft, review, supervision.

Conflicts of interest

The authors declare that they have no competing interests.

Data availability

The data supporting this article have been included in the main text and the supplementary information (SI). Supplementary information: Fig. 1S: (a and b) Nitrogen adsorption–desorption isotherms, (c and d) average pore diameter. Note: (a and c) for cellulose & (b and d) for MC. Fig. 2S: Effect of adsorbent dosage on of the dyes adsorption on MC studied dyes (100 mg L^{-1}), sorbent (1 g L^{-1}), pH = 6 for BG, MG and pH = 10 for CV, MB, at 308 K. Fig. 3S: Adsorption isotherms at different MC dosages ((25–600) mg L^{-1}) initial concentrations, studied dyes (100 mg L^{-1}), sorbent (1 g L^{-1}), pH = 6 for BG, MG and pH = 10 for CV, MB, at 308 K. Fig. 4S: Adsorption isotherms models by MC the nonlinear curve fittings (a) MC-MB, (b)MC-CV, (c) MC-BG and (d) MC-MG. Fig. 5S: Effect of contact time on the removal efficiency of the studied dyes by MC: studied dyes (100 mg L^{-1}), sorbent (1 g L^{-1}), pH = 6 for BG, MG and pH = 10 for CV, MB, at 308 K. Fig. 6S: Kinetic models fittings for the studied dyes adsorption on MC. Fig. 7S: Plot of $\ln K_C$ *vs.* $1/T$ absolute temperature. Fig 8S: (A) Various eluents were used to desorb CV, MB, BG, and MG from the MC adsorbent. (B) Ethanol and HCl in a 1 : 1 ratio served as an eluent for five cycles of adsorption and desorption of CV, MB, BG, and MG. Table 1S: Elemental analysis of the prepared materials. Table 2S: Adsorption kinetics and isotherms nonlinear models. Table 3S: Thermodynamic parameters of the studied adsorption processes. Table 4S: Effect ionic strength on the removal percentages of the studied dyes. See DOI: https://doi.org/10.1039/d5ra03131a.

Acknowledgements

This research has received funding from the Science, Technology & Innovation Funding Authority (STDF) under grant PGSG 48616. This paper is based upon work supported by the Science, Technology & Innovation Funding Authority (STDF) under grant PGSG 48616.

References

1 L. Lin, H. Yang and X. Xu, Effects of water pollution on human health and disease heterogeneity: a review, *Front. Environ. Sci.*, 2022, **10**, 880246.
2 A. Adak, M. Bandyopadhyay and A. Pal, Removal of crystal violet dye from wastewater by surfactant-modified alumina, *Sep. Purif. Technol.*, 2005, **44**(2), 139–144, DOI: 10.1016/j.seppur.2005.01.002.
3 M. Sarabadan, H. Bashiri and S. M. Mousavi, Removal of crystal violet dye by an efficient and low cost adsorbent: Modeling, kinetic, equilibrium and thermodynamic studies, *Korean J. Chem. Eng.*, 2019, **36**(10), 1575–1586, DOI: 10.1007/s11814-019-0356-1.
4 A. Ahmad, S. Hamidah, C. Chuong, *et al.*, Recent Advances in New Generation Dye Removal Technologies: Novel Search of Approaches to Reprocess Waste Water, *RSC Adv.*, 2015, **5**, 30801–30818.
5 A. G. Mostafa, A. I. Abd El-Hamid and M. A. Akl, Surfactant-supported organoclay for removal of anionic food dyes in

batch and column modes: adsorption characteristics and mechanism study, *Appl. Water Sci.*, 2023, **13**(8), 1–24, DOI: 10.1007/s13201-023-01959-6.

6 M. M. Sabzehmeidani, S. Mahnaee, M. Ghaedi, H. Heidari and V. A. L. Roy, Carbon based materials: a review of adsorbents for inorganic and organic compounds, *Mater. Adv.*, 2021, **2**(2), 598–627.

7 F. Rol, M. N. Belgacem, A. Gandini and J. Bras, Recent advances in surface-modified cellulose nanofibrils, *Prog. Polym. Sci.*, 2019, **88**, 241–264.

8 F. Xue, et al., Structural design of a cellulose-based hyperbranched adsorbent for the rapid and complete removal of Cr (VI) from water, *Chem. Eng. J.*, 2021, **417**, 128037.

9 L. Zhao, C. Liang, S. Li and K. Du, Study of tentacle-like cationic macroporous cellulose spherical adsorbent for heavy metals, *J. Cleaner Prod.*, 2021, **303**, 127114.

10 L. S. Silva, et al., Dye anionic sorption in aqueous solution onto a cellulose surface chemically modified with aminoethanethiol, *Chem. Eng. J.*, 2013, **218**, 89–98, DOI: 10.1016/j.cej.2012.11.118.

11 A. M. Yousif, O. F. Zaid and I. A. Ibrahim, Fast and selective adsorption of As(V) on prepared modified cellulose containing Cu(II) moieties, *Arabian J. Chem.*, 2016, **9**(5), 607–615, DOI: 10.1016/j.arabjc.2015.02.004.

12 A. F. Saber, C. C. Chueh, M. Rashad, S. W. Kuo and A. F. M. EL-Mahdy, Thiazolyl-linked conjugated microporous polymers for enhancement adsorption and photocatalytic degradation of organic dyes from water, *Mater. Today Sustain.*, 2023, **23**, 100429, DOI: 10.1016/j.mtsust.2023.100429.

13 W. Zhang, R.-Z. Zhang, Y.-Q. Huang and J.-M. Yang, Effect of the synergetic interplay between the electrostatic interactions, size of the dye molecules, and adsorption sites of MIL-101 (Cr) on the adsorption of organic dyes from aqueous solutions, *Cryst. Growth Des.*, 2018, **18**(12), 7533–7540.

14 A. Ajayaghosh, S. J. George and A. P. H. J. Schenning, Hydrogen-bonded assemblies of dyes and extended π-conjugated systems, *Supramol. Dye Chem.*, 2005, 83–118.

15 A. Kumar, R. R. Ujjwal, A. Mittal, A. Bansal and U. Ojha, Polyacryloyl hydrazide: An efficient, simple, and cost effective precursor to a range of functional materials through hydrazide based click reactions, *ACS Appl. Mater. Interfaces*, 2014, **6**(3), 1855–1865, DOI: 10.1021/am404837f.

16 J. Smits and R. Van Grieken, Synthesis of a chelating cellulose filter with 2,2′-diaminodiethylamine functional groups, *Angew. Makromol. Chem.*, 1978, **72**(1), 105–113, DOI: 10.1002/apmc.1978.050720109.

17 D. Quimica, D. Q. Analitica and D. Barcelona, *Anal. Chim. Acta*, 1987, **151**, 325–329.

18 J. N.Nwabueze, O. Adedirin, S. A. Emmanuel and R. A. Alebiosu, Complexes of Some M(II) Sulphates with Some Hydrazine Derivatives, *Int. J. Chem. Phys. Sci.*, 2013, **1**(6), 406–411.

19 N. Ulusoy Güzeldemırcı, E. Pehlıvan, Z. Halamoğlu and A. Kocabalkanli, 1,3-Tiyazol halkası taşıyan bazı yeni siklohekzilidenhidrazit türevlerinin sentezi ve antiviral etkileri, *Marmara Pharm. J.*, 2016, **20**(2), 207–215, DOI: 10.12991/mpj.20162019913.

20 A. I. Abd-Elhamid, et al., Enhanced removal of cationic dye by eco-friendly activated biochar derived from rice straw, *Appl. Water Sci.*, 2020, **10**, 1–11.

21 M. Thommes, et al., Physisorption of gases, with special reference to the evaluation of surface area and pore size distribution (IUPAC Technical Report), *Pure Appl. Chem.*, 2015, **87**(9–10), 1051–1069, DOI: 10.1515/pac-2014-1117.

22 M. H. Hussin, et al., Physicochemical of microcrystalline cellulose from oil palm fronds as potential methylene blue adsorbents, *Int. J. Biol. Macromol.*, 2016, **92**, 11–19, DOI: 10.1016/j.ijbiomac.2016.06.094.

23 U. P. Agarwal, S. A. Ralph, C. Baez, R. S. Reiner and S. P. Verrill, Effect of sample moisture content on XRD-estimated cellulose crystallinity index and crystallite size, *Cellulose*, 2017, **24**(5), 1971–1984, DOI: 10.1007/s10570-017-1259-0.

24 N. Kasuya, T. Suzuki and A. Sawatari, Studies on the thermal properties and structures of deoxyhalocelluloses, *J. Wood Sci.*, 1999, **45**(2), 161–163, DOI: 10.1007/BF01192334.

25 M. K. Mohamad Haafiz, S. J. Eichhorn, A. Hassan and M. Jawaid, Isolation and characterization of microcrystalline cellulose from oil palm biomass residue, *Carbohydr. Polym.*, 2013, **93**(2), 628–634, DOI: 10.1016/j.carbpol.2013.01.035.

26 M. A. Akl, A. S. El-Zeny, M. A. Hashem, E.-S. R. H. El-Gharkawy and A. G. Mostafa, Flax fiber based semicarbazide biosorbent for removal of Cr (VI) and Alizarin Red S dye from wastewater, *Sci. Rep.*, 2023, **13**(1), 8267.

27 M. A. Akl, A. S. El-Zeny, M. A. Hashem and E. S. R. H. El-Gharkawy, Synthesis, Characterization and Analytical Applications of Chemically Modified Cellulose for Remediation of Environmental Pollutants, *Egypt. J. Chem.*, 2021, **64**(7), 3889–3901, DOI: 10.21608/ejchem.2021.65793.3412.

28 M. A. Akl, A. S. El-Zeny, M. Ismail, M. Abdalla, D. Abdelgelil and A. G. Mostafa, Smart guanyl thiosemicarbazide functionalized dialdehyde cellulose for removal of heavy metal ions from aquatic solutions: adsorption characteristics and mechanism study, *Appl. Water Sci.*, 2023, **13**(6), 1–18, DOI: 10.1007/s13201-023-01948-9.

29 T. A. Yousef, G. M. Abu El-Reash, O. A. El-Gammal and B. M. Sharaa, Characterization, quantum, antibacterial, antifungal and antioxidant studies on Hg(II) and Cd(II) complexes of allyl and ethyl thiosemicarbazides derived from 2-aminothiazole-4-yl acetohydrazide, *Egypt. J. Basic Appl. Sci.*, 2016, **3**(1), 44–60, DOI: 10.1016/j.ejbas.2015.09.005.

30 K. Kuroda, H. Kunimura, Y. Fukaya and H. Ohno, 1H NMR analysis of cellulose dissolved in non-deuterated ionic liquids, *Cellulose*, 2014, **21**(4), 2199–2206, DOI: 10.1007/s10570-014-0271-x.

31 R. D. S. Bezerra, et al., Direct modification of microcrystalline cellulose with ethylenediamine for use as

adsorbent for removal amitriptyline drug from environment, *Molecules*, 2017, **22**(11), DOI: **10.3390/molecules22112039**.

32 M. S. Abdel-Wahed, A. S. El-Kalliny, F. A. Shehata, A. M. Abd El-Aty and T. A. Gad-Allah, One-pot green synthesis of magnetic adsorbent via Anabaena sphaerica and its performance towards Remazol Red dye removal from aqueous media, *Chem. Eng. Sci.*, 2023, **279**(February), 118939, DOI: **10.1016/j.ces.2023.118939**.

33 J. Wang and X. Guo, Adsorption kinetic models: Physical meanings, applications, and solving methods, *J. Hazard. Mater.*, 2020, **390**(January), 122156, DOI: **10.1016/j.jhazmat.2020.122156**.

34 Y. El Maguana, N. Elhadiri, M. Benchanaa and R. Chikri, Activated Carbon for Dyes Removal: Modeling and Understanding the Adsorption Process, *J. Chem.*, 2020, **2020**, 096834, DOI: **10.1155/2020/2096834**.

35 M. Jahandar Lashaki, M. Fayaz, S. Niknaddaf and Z. Hashisho, Effect of the adsorbate kinetic diameter on the accuracy of the Dubinin-Radushkevich equation for modeling adsorption of organic vapors on activated carbon, *J. Hazard. Mater.*, 2012, **241**(242), 154–163, DOI: **10.1016/j.jhazmat.2012.09.024**.

36 K. Sukla Baidya and U. Kumar, Adsorption of brilliant green dye from aqueous solution onto chemically modified areca nut husk, *S. Afr. J. Chem. Eng.*, 2021, **35**(July 2020), 33–43, DOI: **10.1016/j.sajce.2020.11.001**.

37 M. A. Akl, A. G. Mostafa, M. Al-Awadhi, W. S. Al-Harwi and A. S. El-Zeny, Zinc chloride activated carbon derived from date pits for efficient biosorption of brilliant green: adsorption characteristics and mechanism study, *Appl. Water Sci.*, 2023, **13**(12), 1–21, DOI: **10.1007/s13201-023-02034-w**.

38 N. Nasuha, B. H. Hameed and A. T. M. Din, Rejected tea as a potential low-cost adsorbent for the removal of methylene blue, *J. Hazard. Mater.*, 2010, **175**(1–3), 126–132, DOI: **10.1016/j.jhazmat.2009.09.138**.

39 L. Mouni, et al., Removal of Methylene Blue from aqueous solutions by adsorption on Kaolin: Kinetic and equilibrium studies, *Appl. Clay Sci.*, 2018, **153**(March 2017), 38–45, DOI: **10.1016/j.clay.2017.11.034**.

40 N. Somsesta, V. Sricharoenchaikul and D. Aht-Ong, Adsorption removal of methylene blue onto activated carbon/cellulose biocomposite films: Equilibrium and kinetic studies, *Mater. Chem. Phys.*, 2020, **240**(June 2019), 122221, DOI: **10.1016/j.matchemphys.2019.122221**.

41 P. L. Homagai, R. Poudel, S. Poudel and A. Bhattarai, Adsorption and removal of crystal violet dye from aqueous solution by modified rice husk, *Heliyon*, 2022, **8**(4), e09261, DOI: **10.1016/j.heliyon.2022.e09261**.

42 P. P. Kyi, J. O. Quansah, C. G. Lee, J. K. Moon and S. J. Park, The removal of crystal violet from textile wastewater using palm kernel shell-derived biochar, *Appl. Sci.*, 2020, **10**(7), 2251–2263, DOI: **10.3390/app10072251**.

43 R. A. E. G. Mansour, M. G. Simeda and A. A. Zaatout, Removal of brilliant green dye from synthetic wastewater under batch mode using chemically activated date pit carbon, *RSC Adv.*, 2021, **11**(14), 7851–7861, DOI: **10.1039/d0ra08488c**.

44 S. J. Peighambardoust, O. Aghamohammadi-Bavil, R. Foroutan and N. Arsalani, Removal of malachite green using carboxymethyl cellulose-g-polyacrylamide/montmorillonite nanocomposite hydrogel, *Int. J. Biol. Macromol.*, 2020, **159**, 1122–1131, DOI: **10.1016/j.ijbiomac.2020.05.093**.